Magnetic oxide nanowires with strain-controlled uniaxial magnetic anisotropy direction

M. Mathews, R. Jansen, G. Rijnders, J. C. Lodder, and D. H. A. Blank
MESA+ Institute for Nanotechnology, University of Twente, 7500 AE Enschede, The Netherlands
(Received 3 April 2009; published 14 August 2009)

While magnetic nanowires generally have a preferential magnetization direction along the wire axis to minimize magnetostatic energy, it is shown here for epitaxial magnetic oxide nanowires that substrate-induced strain can be used to tailor the magnetic easy axis in any direction. $La_{0.67}Sr_{0.33}MnO_3$ (LSMO) nanowires were prepared by pulsed laser deposition of LSMO thin films on $NdGaO_3$ (NGO) substrates of two different orientations [$NGO(110)_o$ and $NGO(010)_o$], followed by patterning into arrays of nanowires by laser interference lithography. The uniaxial compressive strain from the substrate induces a strong uniaxial magnetic anisotropy in the LSMO that dominates the anisotropy. Hence, one obtains LSMO nanowires having a magnetic easy axis that can lie in any direction, including perpendicular to the wire axis. In marked contrast, similar nanowires on $SrTiO_3(001)$ substrates without significant uniaxial strain exhibit the usual preferential magnetization direction along the wire axis, as dictated by magnetostatic shape anisotropy. The tunable magnetic anisotropy direction is a useful feature for applications of magnetic nanowires in magnetic memory, sensor, and logic devices.

DOI: 10.1103/PhysRevB.80.064408 PACS number(s): 75.70.−i, 68.55.−a, 81.15.Fg, 75.60.−d

I. INTRODUCTION

Magnetic oxides attract considerable interest because of their rich variety of properties, including colossal magnetoresistance,[1] half-metallic ferromagnetism,[2,3] magnetism in oxide semiconductors with dilute doping,[4,5] as well as electrically driven reversible resistance switching.[6] The half-metallic character of some magnetic oxides leads to a very high spin-polarization of the conduction electrons, in theory 100%. Indeed, a spin-polarization of 95% was observed for $La_{0.67}Sr_{0.33}MnO_3$ (LSMO) in tunneling experiments.[3] Together with the ability to combine these materials in epitaxial fashion with other oxides such as superconductors,[7] semiconductors,[8] ferroelectrics[9,10] and multiferroics,[11] this gives a unique playground for controlled fundamental studies as well as application of magnetic oxides in magnetic memory, sensor and logic devices. By default, such devices involve nanoscale elements, with the nanowire-based magnetic racetrack memory[12] as the most salient recent example. Hence, the ability to control and tune the magnetic properties of oxide nanomagnets is an important topic.

In general, a magnetic nanowire has a magnetization that points preferentially along the wire axis, as this reduces the magnetostatic energy.[13,14] The strength of this so-called magnetic shape anisotropy increases as the aspect ratio of the magnetic element increases, and is therefore often the dominant source of magnetic anisotropy in nanowires. The epitaxial growth of magnetic oxides on various single crystals allows one to introduce an additional source of anisotropy due to substrate-induced strain. This has been demonstrated for thin films of various magnetic oxides, including LSMO, for which the magnetic properties are sensitive to strains imposed by the lattice mismatch between the film and the substrate.[15–22]

Only a few studies have so far been done on patterned complex magnetic oxides.[23–25] Submicron LSMO islands of different aspect ratio on $LaAlO_3$ substrate were reported to have characteristic multidomain structure with perpendicular orientation,[23] influenced by the compressive strain from the substrate. Recently, magnetic oxide nanostructures embedded in a paramagnetic matrix prepared by electron beam lithography and ion implantation have been also reported.[25] In this letter, we report the control of the magnetic anisotropy in epitaxial LSMO nanowires on NGO substrates using strain engineering. We show that the uniaxial substrate-induced strain can create a large uniaxial magnetic anisotropy in the LSMO nanowires that is strong enough to overcome the magnetic shape anisotropy and dominates the magnetic anisotropy of the nanowires. Consequently, nanowires are obtained with the magnetic easy axis oriented at any angle with respect to the wire axis, even perpendicular to it.

II. EXPERIMENT

The LSMO is grown using pulsed laser deposition (PLD), which is known as a powerful technique for making thin films with atomically smooth surface and interfaces, atomically regulated thickness, and controlled epitaxial strain caused by the substrate. As substrate we choose NGO of two different orientations, namely, $(110)_o$ and $(010)_o$, for which the LSMO is subjected to strain values that are unequal for the two in-plane crystal directions. The subscript "o" denotes orthorhombic metric. LSMO films were deposited at a substrate temperature of 750 °C from a stoichiometric target in an oxygen background pressure of 0.35 mbar and a laser fluence of 3 J/cm^2. The target to substrate distance was fixed at 4 cm. After LSMO deposition, the films were cooled to room temperature with 10 °C/min ramp rate in 1 bar of oxygen gas. The crystal structure of the films was examined using x-ray diffraction (XRD) two-theta scans. The thickness of the films was determined using low-angle XRD while the surface morphology was analyzed by Atomic Force Microscopy (AFM). In order to pattern arrays of LSMO nanowires, the epitaxial LSMO films are spin coated with diluted photoresist (Arch 907 aka Olin) and exposed in a laser interfer-

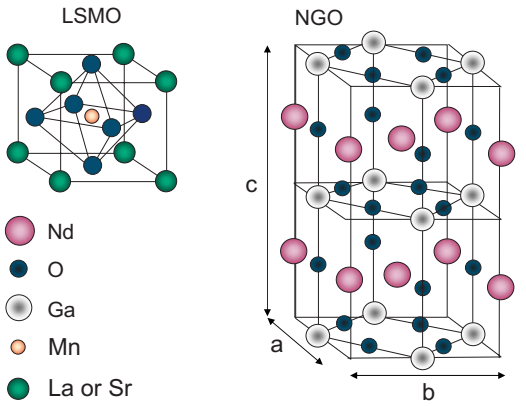

FIG. 1. (Color) Schematic diagrams of the crystal unit cell of $La_{0.67}Sr_{0.33}MnO_3$ (LSMO) and $NdGaO_3$ (NGO) with the orthorhombic *a*, *b*, and *c* axis indicated.

ence lithography (LIL) setup.[26] Then the sample is etched by argon ion milling, followed by ultrasonic cleaning in acetone to remove the photoresist. After optimizing the LIL exposure time and the etching time, LSMO nanowires of different dimensions and periodicity can be obtained. We report here on arrays of wires with a 300 nm width and 600 nm periodicity. The nanowire length is approximately 4.5 mm, with the array of wires covering a surface area of 4.5 by 4.5 mm. Magnetic measurements were done using a vibrating sample magnetometer (VSM) at room temperature, on nanowires as well as on continuous films for comparison. Below we shall first describe the properties of the latter.

III. RESULTS AND DISCUSSION

A. Structure

In order to understand the expected strain of the LSMO lattice on NGO substrates of different orientations, we first describe the crystal structure of LSMO and NGO, for which the unit cells are schematically represented in Fig. 1. LSMO has pseudocubic crystal structure with bulk lattice parameter=3.88 Å. The orthorhombic crystal structure of NGO (with lattice parameters a=5.426 Å, b=5.496 Å, and c=7.706 Å) can also be described in the pseudocubic space group, in which the (100) pseudocubic direction corresponds to the (110) orthorhombic direction, and the average pseudocubic lattice parameter, a1, is related to the orthorhombic unit cell by $a \sim \sqrt{2}$ a1, $b \sim \sqrt{2}$ a1, and $c \sim 2$ a1. The growth orientations of LSMO on $NGO(110)_o$ and $(010)_o$ substrates are different. Figures 2(a)–2(c) shows how LSMO grows on a $NGO(110)_o$ substrate having its surface terminated with the GaO_2 crystal plane. Figure 2(a) shows the top view of the GaO_2 termination plane and (b) illustrates how the LSMO cubic lattice fits onto it. In Fig. 2(c), the stacking of the LSMO on the substrate is depicted as a side view. Using the LSMO and NGO lattice parameters, the lattice mismatch of the film can be calculated and the expected strain can be obtained for an LSMO film grown in epitaxial mode. We obtain a compressive strain of 0.70% along the in-plane "*c*" axis ([001] direction) of NGO $(110)_o$, while there is a smaller compressive strain of 0.47% in the in-plane direction perpendicular to it.

Similarly, Figs. 2(d)–2(f) shows how LSMO grows on $NGO(010)_o$ substrates. The most salient feature is that the LSMO grows with its [011] axis perpendicular to the surface

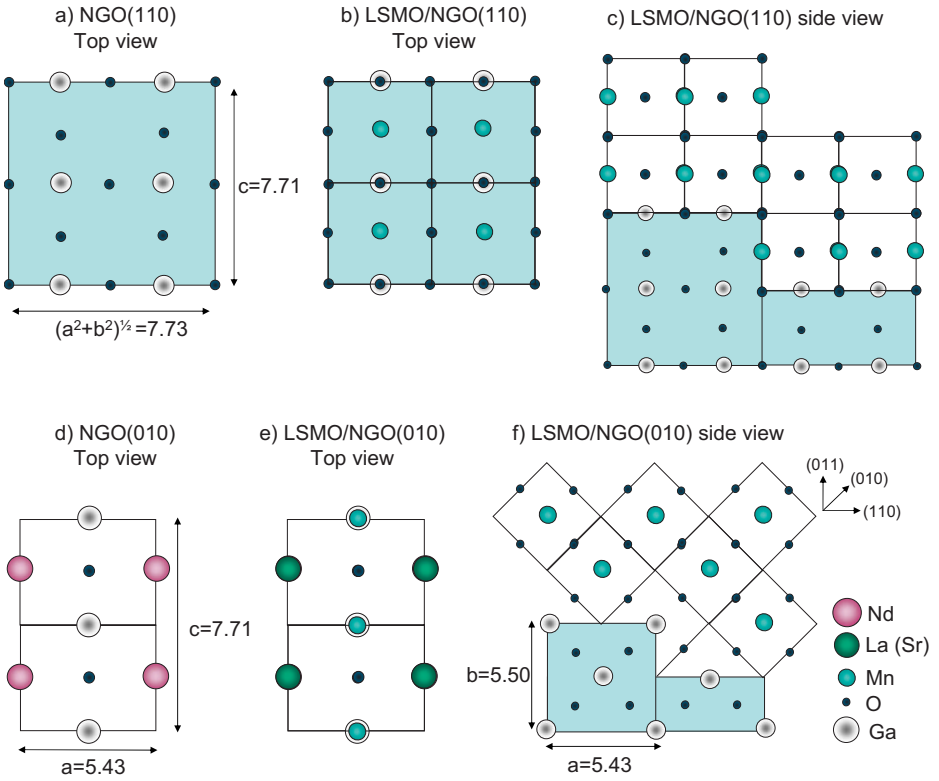

FIG. 2. (Color) (a)–(c) LSMO on $NGO(110)_o$. Top view of the GaO_2 terminated surface of $NGO(110)_o$ without (a) and with (b) the first atomic layer of LSMO overlaid. (c) Side view of the LSMO stacking on a $NGO(110)_o$ substrate. (d)–(f) LSMO on $NGO(010)_o$. Top view of the surface of $NGO(010)_o$ without (d) and with (e) the first atomic layer of LSMO overlaid. (f) Side view of the LSMO stacking on a $NGO(010)_o$ substrate. Arrows indicate the LSMO lattice orientations $(011)_{pc}$, $(010)_{pc}$, and $(110)_{pc}$, where the subscript "pc" denotes the crystal reflections with respect to the pseudocubic crystal system of LSMO.

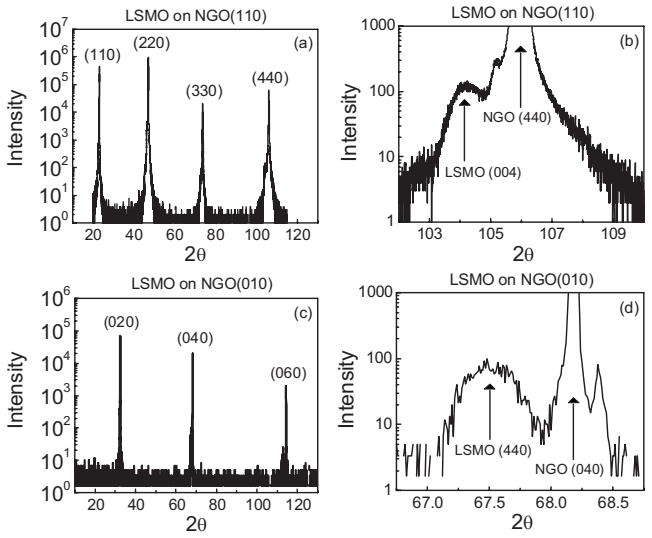

FIG. 3. XRD 2-theta scans of, respectively, $NGO(110)_o$ with a 18 nm LSMO film [(a) and (b)], and $NGO(010)_o$ with a 19 nm LSMO film [(c) and (d)], where the right hand panels (b) and (d) show a section of the two-theta scan zoomed in around the fourth order peak of the substrate. The labeled main reflections in (a) and (c) are due to the substrate, while the reflections from the LSMO film are identified by labels in the right hand panels.

[i.e., the LSMO cube is rotated by 45° in the out of plane direction compared to the case of Fig. 2(c)]. The expected values of the (compressive) lattice strains of LSMO in this case are 1.11% along the [100] in-plane direction and 0.70% in the [001] in-plane direction. For both substrates, the expected strains in the two different in-plane directions are unequal, which, as shown below, leads to a uniaxial in-plane magnetic anisotropy in the LSMO.

Before film deposition, the $NGO(010)_o$ substrates were annealed at 950 °C for 1 h in oxygen flow of 1 bar in order to get a clean and well-ordered surface with straight terraces. For $NGO(110)_o$, before annealing, the substrates were etched in a modified BHF solution for 30 s in order to obtain a GaO_2 surface termination. Surface morphology of the LSMO films characterized by AFM reveals that the films grow smooth and the substrate steps are reproduced on the film surface. The crystal structure of the LSMO films was analyzed by XRD (Fig. 3). The two-theta XRD scan of a representative LSMO film of 15 nm thickness on a $NGO(110)_o$ substrate shows only the peaks corresponding to the $(00l)$ orientations of the film, confirming its crystallinity. Similarly, LSMO grown on $NGO(010)_o$ shows reflections corresponding to the $(hk0)$ orientations, which confirms the crystallinity, but also the rotated growth orientation as described above and shown in Fig. 2(f). The out of plane lattice parameter deduced from these two-theta XRD measurements is 3.906 ± 0.003 Å for $LSMO/NGO(110)_o$ and 5.546 ± 0.004 Å for $LSMO/NGO(010)_o$, corresponding to an out of plane tensile strain 0.67% and 1.1%, respectively.

To determine the in-plane lattice parameters, XRD reciprocal space mapping was carried out on a 25 nm thick LSMO film on $NGO(110)_o$, see Fig. 4. The *hl* scan and *kl* scan were measured, respectively, around the $(204)_{pc}$ and $(024)_{pc}$ reflections, and show two separate peaks associated with the

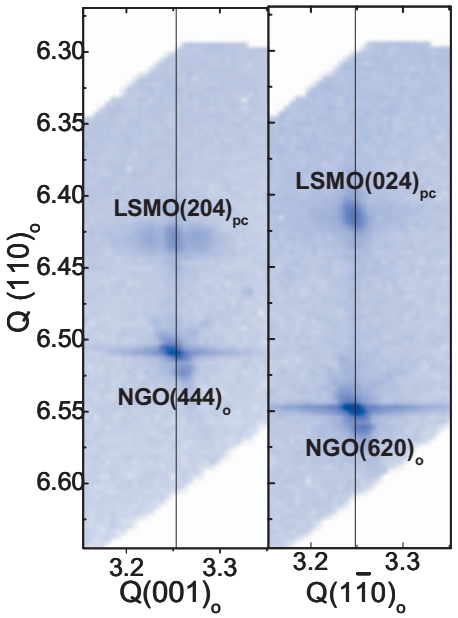

FIG. 4. (Color) (Left panel) XRD *hl* scan of $LSMO/NGO(110)_o$ around the $(204)_{pc}$ reflection. The in-plane *h* values associated with the NGO and LSMO peak are identical, as indicated by the vertical solid line. (Right panel) XRD *kl* scan of the same film around $(024)_{pc}$ reflection. The in-plane *k* values associated with the NGO and LSMO peak are also identical, as indicated by the vertical solid line.

NGO substrate and the LSMO film due to their different out-of-plane lattice parameters (*l* direction or $Q(110)_o$). In addition, the *hl* scan provides selective information about one in-plane lattice parameter [*h* direction or $Q(001)_o$], which is seen to be identical for LSMO film and NGO substrate. The *kl* scan provides selective information about the other, orthogonal in-plane lattice parameter [*k* direction or $Q(1\bar{1}0)_o$], which is also found to be identical for LSMO film and NGO substrate. Hence, we conclude that the in-plane lattice of the LSMO film matches the in-plane lattice of the substrate, implying epitaxial growth and hence the expected uniaxial strain.

B. Magnetic anisotropy of LSMO thin films on NGO

From magnetization curves taken with the field *H* applied in different directions, we find that all films have in-plane magnetization direction, i.e., the direction perpendicular to the film is a magnetic hard axis. In order to study in detail the magnetic anisotropy in the plane of the films, hysteresis loops were taken at different in-plane field directions with intervals of 5°, from which we also obtain the magnetic remanence (i.e., the remanent magnetization at $H=0$). Figure 5(a) shows representative data for a 18 nm LSMO film on $NGO(110)_o$. The curve taken in the $[1\bar{1}0]$ direction of the NGO substrate shows typical easy axis behavior with sharp magnetization switching at small fields and large remanence, while for the field applied in the [001] in-plane direction the film shows very little remanence and much larger saturation field typical for a magnetic hard axis. Figure 5(b) shows the

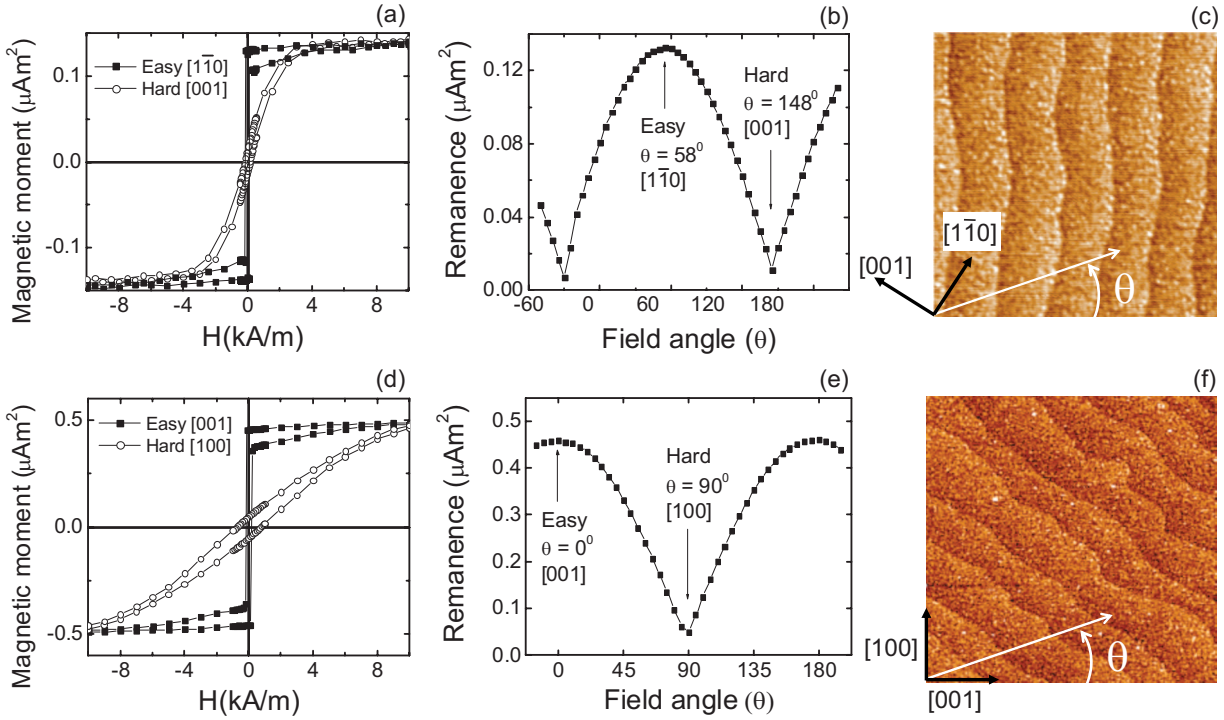

FIG. 5. (Color) (a) Magnetic moment versus applied magnetic field H for a 18 nm thick LSMO film grown on NGO$(110)_o$, measured along the two in-plane crystal directions as indicated. (b) Remanence versus in-plane field angle for the same film. Arrows denote easy and hard directions. (c) Corresponding AFM image (1 μm$\times$1 μm) of the same film, with the two in-plane crystal directions indicated by black arrows, and the angle θ at which the magnetic field is applied defined with respect to the edge of the substrate, as indicated in white. (d)–(f) show a similar set of data for a 50 nm LSMO film on a NGO$(010)_o$ substrate, with an AFM image of 2 μm$\times$2 μm. The gray scale in the AFM images ranges from 0 to 2 nm. All data was taken at room temperature.

extracted magnetic remanence plotted against the in-plane field angle (θ), measured from one edge of the sample as defined in the AFM image shown in Fig. 5(c). The remanence is found to oscillate with a periodicity of 180°, which implies a uniaxial magnetic anisotropy. The highest remanence value occurs around θ=58° corresponding to the in-plane [1$\bar{1}$0] direction. The lowest remanence is at θ=148° (in-plane [001] direction). We thus find that the magnetic easy and hard axis lie along the [1$\bar{1}$0] and [001] in-plane crystal directions, respectively.

The same result is obtained for LSMO on NGO$(010)_o$ substrates, for which a similar set of data is presented in Figs. 5(d)–5(f) for a 50 nm thick LSMO film. Here θ is defined as the angle between the applied field direction and the [001] NGO crystal direction. Again there is a pronounced oscillation of the magnetic remanence with periodicity of 180°, with the highest remanence at $\theta\sim$0° (in-plane [001] direction) and the lowest remanence at $\theta\sim$90° (in-plane [100] direction). Thus, also for this substrate orientation there is a uniaxial magnetic anisotropy, in this case with easy axis along [001] and hard axis along the [100] in-plane direction. As outlined above, the compressive strain induced in the LSMO by both of these NGO substrates is different in the two in-plane directions. This modifies the magnetocrystalline anisotropy and results in a uniaxial magnetic anisotropy. Compared to LSMO films on STO substrates,[21] for LSMO on NGO we obtain a much larger amplitude of the oscillation of the remanence, which almost reaches zero for the magnetic hard axis direction. We also note that the in-plane magnetic easy axis does not coincide with the orientation of the steps and terraces on the film surface [see AFM images in Figs. 5(c) and 5(f)]. Therefore, the step-induced uniaxial anisotropy, previously observed for LSMO on vicinal STO substrates,[21] is weak compared to the strong strain-induced anisotropy.

C. Magnetic anisotropy of LSMO nanowires on NGO

Next, we exploit the strain-induced magnetic anisotropy to manipulate the magnetization direction of magnetic nanowires. Figure 6 shows data obtained on a representative LSMO nanowire sample on a NGO$(110)_o$ substrate. The nanowires have a width of 300 nm, length of 4.5 mm, height (film thickness) of 20 nm, and a periodicity of 600 nm, while the axis of the wires is along one edge of the substrate [i.e., along θ=90°, as can be seen in the AFM image of Fig. 6(c)]. The magnetic hysteresis loop [Fig. 6(a)] taken for θ=60° ([1$\bar{1}$0] direction) shows typical easy axis behavior with relatively sharp magnetization switching and large remanence, while for the field applied at $\theta\sim$150° ([001] direction) the nanowires show smaller remanence and hysteresis. Figure 6(b) shows that the remanence oscillates with the in-plane field angle θ with a periodicity of 180°, implying a uniaxial magnetic anisotropy. However, the most salient feature is that the highest remanence value occurs around θ=58°, i.e., when the magnetic field is applied at an angle of about 30°

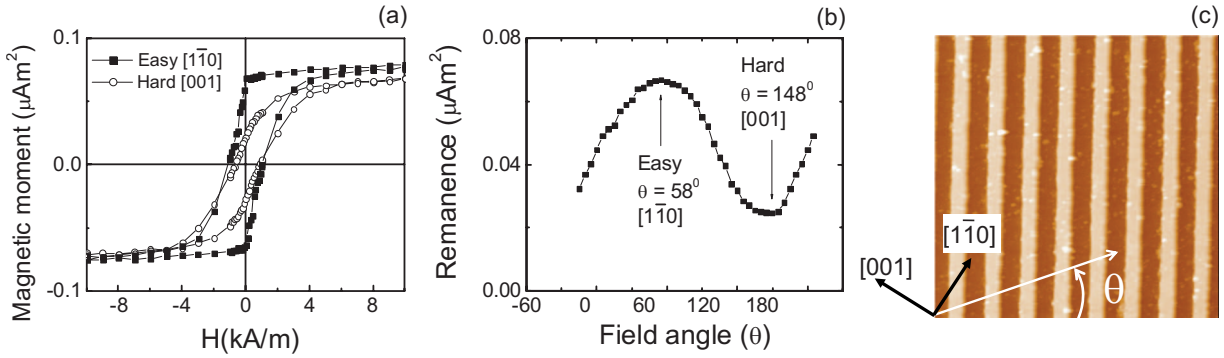

FIG. 6. (Color) Similar set of data as in Figs. 5(a)–5(c), but now for LSMO nanowires on a NGO$(110)_o$ substrate. The nanowires have a width of 300 nm, length of 4.5 mm, height (film thickness) of 20 nm, and a periodicity of 600 nm, while the axis of the wires is along one edge of the substrate (i.e., along θ=90°). The definition of the field angle θ and crystal axis orientation is the same as for the continuous film shown in Figs. 5(a)–5(c). The AFM image size is 5 μm×5 μm. All data was taken at room temperature.

with respect to the long axis of the nanowires. Similarly, the magnetic hard axis is not perpendicular to the nanowires, as it would be if magnetic shape anisotropy would dominate. Rather, the hard axis is at $\theta \sim 148°$, which is about 60° away from the nanowire axis. In fact, the magnetic easy and hard axes of the nanowires coincide with the in-plane crystal directions, [1$\bar{1}$0] and [001], respectively. We thus find that the LSMO nanowires have a uniaxial magnetic anisotropy direction that is determined by the strain induced by the substrate, and not by the magnetic shape anisotropy of the wires. Obviously, the large uniaxial magnetic anisotropy induced by the strain is essential.

Given that the magnetic anisotropy of the nanowires is determined by the in-plane crystal orientation, it becomes possible to create nanowires with a magnetic easy axis at any angle with the nanowire axis. We demonstrate this for the extreme case of nanowires having a magnetic easy axis perpendicular to the wire axis. For that purpose, LSMO films on NGO$(010)_o$ substrates were patterned into nanowires oriented along the [100] in-plane crystal direction [see AFM image in Fig. 7(c)]. The wires have a width of 300 nm, length of 4.5 mm, height of 25 nm, and a periodicity of 600 nm. Figures 7(a) and 7(b) shows the in-plane hysteresis loops and extracted remanence versus in-plane field angle, from which we can see that the magnetic easy axis lies along the [001] direction ($\theta \sim 0°$). Indeed, this is perpendicular to the axis of the nanowires. The wires also exhibit a uniaxial anisotropy with the magnetic hard axis in the [100] in-plane crystal direction ($\theta \sim 90°$), which is along the nanowire axis.

D. Magnetic anisotropy of LSMO nanowires on STO

For comparison we have also prepared LSMO nanowires with similar dimensions on $SrTiO_3$ (STO) substrates, using the same fabrication method. On STO(001), the epitaxial LSMO films have equal in-plane tensile strain of 0.64% in both the orthogonal in-plane directions. Thus, in this case the LSMO lacks strain-induced magnetocrystalline anisotropy in the film plane. Therefore, the magnetic easy axis of nanowires on STO is expected to be along the long axis of the wires, as dictated by the magnetostatic shape anisotropy. This conventional behavior is indeed observed [see Fig. 8], showing that a significant magnetostatic anisotropy is indeed present in such LSMO nanowires (we note that the observed uniaxial behavior is not due to the (weak) step-induced uniaxial anisotropy previously observed in LSMO films on vicinal STO at room temperature,[21] since the nanowires were patterned at an angle with the surface steps, which for the sample of Fig. 8 were oriented along the [110] direction).

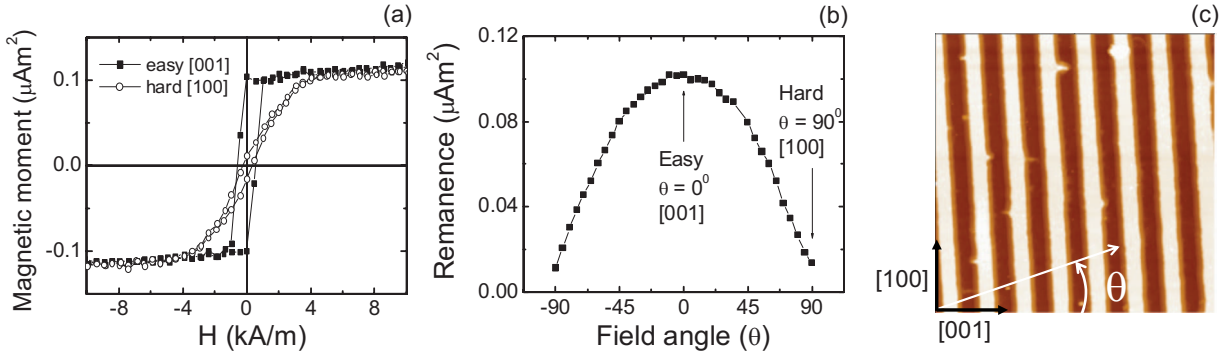

FIG. 7. (Color) Similar set of data as in Figs. 5(d)–5(f), but now for LSMO nanowires on a NGO$(010)_o$ substrate. The nanowires have a width of 350 nm, length of 4.5 mm, height (film thickness) of 25 nm, and a periodicity of 600 nm, while the axis of the wires is along one edge of the substrate (i.e., along θ=90°). The definition of the field angle θ and crystal axis orientation is the same as for the continuous film shown in Figs. 5(d)–5(f). The AFM image size is 5 μm×5 μm. All data was taken at room temperature.

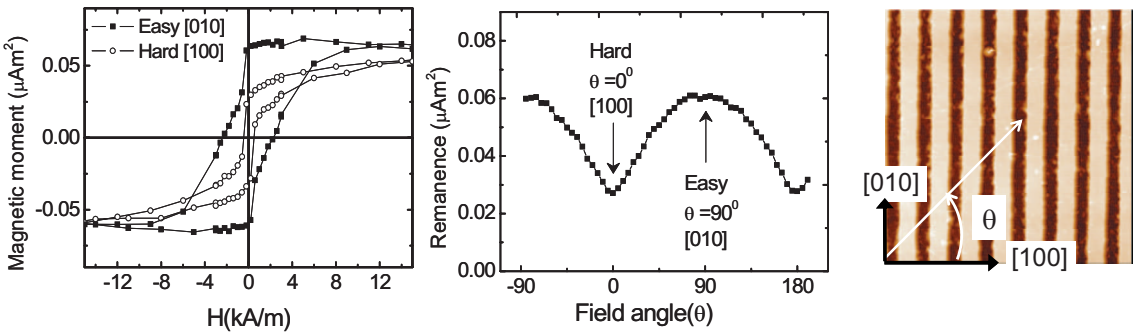

FIG. 8. (Color) Similar set of data as in Fig. 6, but now for LSMO nanowires on a STO(001) substrate. The nanowires have a width of 420 nm, length of 4.5 mm, height (film thickness) of 26 nm, and a periodicity of 600 nm, while the long axis of the wires is along one edge of the substrate (i.e., along θ=90°). The definition of the field angle θ and crystal axis orientation is depicted in the AFM image (5 μm $\times$5 μm) on the right. All data was taken at room temperature.

E. Analysis

For a more quantitative comparison, we estimate the anisotropy energy associated with the uniaxial strain induced by the NGO substrate, and the magnetostatic anisotropy energy of the nanowires. For the latter, we approximate the wire as a spheroid (rod) or rectangular prism, with semimajor axis "*c*" along the length of the wire, the minor axis "*a*" along the width of the wire, and the other minor axis "*b*" along the height (thickness) of the wire. The magnetostatic anisotropy constant, K_{static}, corresponding to the in-plane anisotropy, is then given by[27] $K_{\text{static}}=(1/2)\mu_0 M_s^2\ (N_a-N_c)$, where M_s is the saturation magnetization of LSMO (measured to be 360 kA/m at room temperature). The demagnetization factors N_a and N_c along the two in-plane directions can be calculated[28] for the given dimensions of the nanowires (a=420 nm, b=26 nm, and c=4.5 mm), yielding N_a=0.08 and $N_c=6.6\times10^{-6}$. This gives $K_{\text{static}}=6.51\times10^3$ J/m^3, which is sufficient to force the magnetic easy axis of the nanowires on STO along the wire axis.

For the strain-induced anisotropy, we start from the general expression for the magnetoelastic energy due to strain in cubic materials, given by:[28,29]

$$E=-(3/2)\lambda_{100}\sigma(\alpha_1^2\gamma_1^2+\alpha_2^2\gamma_2^2+\alpha_3^2\gamma_3^2)-3\lambda_{111}\sigma(\alpha_1\alpha_2\gamma_1\gamma_2+\alpha_2\alpha_3\gamma_2\gamma_3+\alpha_3\alpha_1\gamma_3\gamma_1). \quad (1)$$

Here, α_1, α_2, and α_3 are the direction cosines of the magnetization and γ_1, γ_2, and γ_3 are direction cosines of the tension (σ) in the ferromagnetic body ($\sigma=Y\varepsilon$, with Y the young's modulus, and ε the strain vector $(\varepsilon_1,\varepsilon_2,\varepsilon_3)$ with magnitude $|\varepsilon|$), and λ_{100} and λ_{111} are the magnetostriction constants in the [100] and [111] directions, respectively. The magnetoelastic anisotropy energy K_{elastic} associated with the strain induced by the NGO substrate is then obtained as the energy difference between magnetization along the in-plane axis 1 ($\alpha_1=1$, $\alpha_2=0$, $\alpha_3=0$) and the orthogonal in-plane axis 2 ($\alpha_1=0$, $\alpha_2=1$, $\alpha_3=0$), which gives $K_{\text{elastic}}=-(3/2)\lambda_{100}\ \sigma\ (\gamma_1^2-\gamma_2^2)$ or equivalently $K_{\text{elastic}}=-(3/2)\ \lambda_{100}\ Y\ |\varepsilon|\ (\varepsilon_1^2-\varepsilon_2^2)/|\varepsilon|^2$. We consider the case of the LSMO on NGO(110), with in-plane strain parameters $\varepsilon_1=-0.7\%$, $\varepsilon_2=-0.47\%$ and out-of plane strain $\varepsilon_3=+0.67\%$, as determined from the XRD results. A value of $Y=4.5\times10^{11}$ J/m^3 was used for the Young's modulus.[30,31] The magnetostriction constant λ_{100} was reported[30] to be between 2.2×10^{-5} and $(7-10)\times10^{-5}$. Using the lowest value (2.2×10^{-5}), we obtain a lower bound for K_{elastic} of 3.7×10^4 J/m^3. This is about an order of magnitude larger than the magnetostatic anisotropy energy of the nanowires, consistent with the observation that strain controls the magnetic anisotropy of the LSMO nanowires on NGO substrates.

IV. CONCLUSION

Thus for nanowires on NGO substrates, the magnetic anisotropy due to the substrate-induced lattice strain is strong enough to dominate over the shape anisotropy, and allows the magnetic easy axis of the nanowires to lie in any direction, even perpendicular to the wires. Strain engineering in epitaxial oxide nanowires via a suitable choice of substrate is therefore a viable approach to manipulate and tune the magnetic properties of nanowires and create a uniaxial magnetic anisotropy in any direction. This is a very useful feature for applications of magnetic nanowires in magnetic memory, sensor and logic devices.

ACKNOWLEDGMENTS

We acknowledge financial support from NanoNed, the nanotechnology network in the Netherlands, and from the Dutch Technology Foundation (STW).

[1] A.-M. Haghiri-Gosnet and J.-P. Renard, J. Phys. D **36**, R127 (2003).
[2] J.-H. Park, E. Vescovo, H.-J. Kim, C. Kwon, R. Ramesh, and T. Venkatesan, Nature (London) **392**, 794 (1998).
[3] M. Bowen, M. Bibes, A. Barthélémy, J. P. Contour, A. Anane, Y. Lemaitre, and A. Fert, Appl. Phys. Lett. **82**, 233 (2003).
[4] Y. Matsumoto, M. Murakami, T. Shono, T. Hasegawa, T. Fukumura, M. Kawasaki, P. Ahmet, T. Chikyow, S.-ya Koshihara, and H. Koinuma, Science **291**, 854 (2001).
[5] S. A. Chambers, Surf. Sci. Rep. **61**, 345 (2006).
[6] T. Fujii, M. Kawasaki, A. Sawa, H. Akoh, Y. Kawazoe, and Y. Tokura, Appl. Phys. Lett. **86**, 012107 (2005).
[7] J. Orenstein and A. J. Millis, Science **288**, 468 (2000).
[8] F. M. Postma, R. Ramaneti, T. Banerjee, H. Gokcan, E. Haq, D. H. A. Blank, R. Jansen, and J. C. Lodder, J. Appl. Phys. **95**, 7324 (2004).
[9] C. H. Ahn, K. M. Rabe, and J.-M. Triscone, Science **303**, 488 (2004).
[10] E. Y. Tsymbal and H. Kohlstedt, Science **313**, 181 (2006).
[11] M. Gajek, M. Bibes, S. Fusil, K. Bouzehouane, J. Fontcuberta, A. Barthélémy, and A. Fert, Nature Mater. **6**, 296 (2007).
[12] S. S. P. Parkin, M. Hayashi, and L. Thomas, Science **320**, 190 (2008).
[13] A. Aharoni, *Introduction to the Theory of Ferromagnetism* (Clarendon Press, Oxford, 1996).
[14] R. P. Cowburn, J. Phys. D **33**, R1 (2000).
[15] C. Kwon, M. C. Robson, K.-C. Kim, J. Y. Gu, S. E. Lofland, S. M. Bhagat, Z. Trajanovic, M. Rajeswari, T. Venkatesan, A. R. Kratz, R. D. Gomez, and R. Ramesh, J. Magn. Magn. Mater. **172**, 229 (1997).
[16] Y. Suzuki, H. Y. Hwang, S-W. Cheong, T. Siegrist, R. B. van Dover, A. Asamitsu, and Y. Tokura, J. Appl. Phys. **83**, 7064 (1998).
[17] K. Steenbeck and R. Hiergeist, Appl. Phys. Lett. **75**, 1778 (1999).
[18] T. W. Olson, J. M. W. Olson, A. Scholl, and Y. Suzuki, J. Appl. Phys. **95**, 7354 (2004).
[19] P. Lecoeur, P. L. Trouilloud, X. Gang, A. Gupta, G. Q. Gong, and X. W. Li, J. Appl. Phys. **82**, 3934 (1997).
[20] J. Dho, Y. N. Kim, Y. S. Hwang, J. C. Kim, and N. H. Hur, Appl. Phys. Lett. **82**, 1434 (2003).
[21] M. Mathews, F. M. Postma, J. C. Lodder, R. Jansen, G. Rijnders, and D. H. A. Blank, Appl. Phys. Lett. **87**, 242507 (2005).
[22] T. Taniuchi, H. Kumigashira, M. Oshima, T. Wakita, T. Yokoya, M. Kubota, and K. Ono, Appl. Phys. Lett. **89**, 112505 (2006).
[23] Y. Wu, Y. Matsushita, and Y. Suzuki, Phys. Rev. B **64**, 220404 (2001).
[24] R.-W. Li, T. Kanki, H.-A. Tohyama, M. Hirooka, H. Tanaka, and T. Kawai, Nanotechnology **16**, 28 (2005).
[25] Y. Takamura, R. V. Chopdekar, A. Scholl, A. Doran, J. A. Liddle, B. Harteneck, and Y. Suzuki, Nano Lett. **6**, 1287 (2006).
[26] R. Murillo, H. A. van Wolferen, L. Abelmann, and J. C. Lodder, Microelectron. Eng. **78-79**, 260 (2005).
[27] B. D. Cullity, *Introduction to Magnetic Materials* (Addison-Wesley, Reading, 1972).
[28] A. Aharoni, J. Appl. Phys. **83**, 3432 (1998).
[29] S. Chikazumi, *Physics of Magnetism* (John Wiley & Sons, New York, 1964), p. 183.
[30] K. Steenbeck, T. Habisreuther, C. Dubourdieu, and J. P. Sénateur, Appl. Phys. Lett. **80**, 3361 (2002).
[31] C. M. Xiong, J. R. Sun, and B. G. Shen, Solid State Commun. **134**, 465 (2005).